MODELING THE CSEM RESPONSE OF UPHEAVAL DOME

An Undergraduate Research Scholars Thesis

by

ANDRÉA DARRH

Submitted to the Undergraduate Research Scholars program at
Texas A&M University
in partial fulfillment of the requirements for the designation as an

UNDERGRADUATE RESEARCH SCHOLAR

Approved by Research Advisor: Dr. Mark E. Everett

May 2017

Major: Geophysics

TABLE OF CONTENTS

ABSTRACT

Modeling the CSEM Response of Upheaval Dome

Andréa Darrh
Department of Geology and Geophysics
Texas A&M University

Research Advisor: Dr. Mark E. Everett
Department of Geology and Geophysics
Texas A&M University

There are currently two different theories for the formation of Upheaval Dome, an enigmatic circular geological formation comprising a tilted rim structure that encloses a central uplifted region. The first theory is that Upheaval Dome, located in Canyonlands National Park, Utah, was formed as a result of uplift caused by the diapiric rising of the buoyant Paradox Salt through the overlaying strata. The second theory is that the formation was caused by a meteorite impact. The objective of this project is to develop geoelectrical models corresponding to each of the two suggested explanations of Upheaval Dome. Starting with analytic solutions of the governing Maxwell equations, as found in *Ward & Hohmann* [1987], *Everett* [1990], *Kauahikaua* [1978], *Ryu et al.* [1970], and *Morrison et al.* [1969], software is developed based on an impedance recursion equation that can accurately simulate the response of a layered geoelectrical model to transient controlled-source electromagnetic (CSEM) excitation. With this analytic equation it will be possible to further develop a 3-D finite element numerical code that will be used to test and evaluate geological models representing a variety of possible subsurface conditions beneath Upheaval Dome. The best-fitting models can be validated through geophysical field work with the intent of resolving subtle resistivity contrasts between deeper

layers in the model. With this application, the range of possible uses for terrestrial CSEM will be expanded to geological structural mapping in rugged, highly resistive terrains, and it will be possible to provide some insight to which of the candidate geological process that resulted in the formation of Upheaval Dome.

ACKNOWLEDGEMENTS

I would like to thank my faculty advisor, Dr. Mark Everett, for his guidance through this project and my mother and father, Cheryl and Edward Darrh, for their love and support and their advice to always keep moving forward.

CHAPTER I

INTRODUCTION

Upheaval Dome is a large, circular structure in Canyonlands National Park, Utah with a diameter of ~5 km [*Kriens et al*., 1999]. The cause of the formation of Upheaval Dome is contested. *Jackson* [1998] suggested that the structure was caused by a salt diapir that has subsequently pinched off and eroded away, citing evidence of growth throughout the last 20 Myr. *Kriens et al.* [1999] proposed that the absence of limestone and black shales on the surface, which would have been carried to the surface along with the salt and would not have been as easily eroded away, argues against the salt-diapir theory. *Kanbur et al.* [2000] found that seismic reflections from the Paradox Salt layer suggest that salt is not present within 1100 m of the surface, with the salt layer characterized by an uplift of ~100 m at that depth. This implies only ~100 m maximum uplift at the surface, conflicting with the exposed uplift of 250 m in the structure and, moreover, since deformation decreases with depth, this is an indicator of external pressure rather than internal.

The difficulty of determining the origin of Upheaval Dome has largely been due to the enigmatic topography and relative inaccessibility of the area. By using a stationary, grounded long wire source, it will be possible to collect CSEM data at the depths that are needed to obtain a potentially decisive geoelectrical image of the subsurface structure. The purpose of this project is to develop representative geological models corresponding to the major theories about the origin of Upheaval Dome, and to evaluate their response using a point-dipole solution. This will motivate geophysical field work to confirm which, if any, of the models is explained by the

observations. Using this technique, it will introduce new uses for CSEM in structural geological mapping within resistive terrains and also provide insight to the origin of Upheaval Dome.

CHAPTER II

METHODS

In order to develop plausible geoelectrical models corresponding to the geologic scenarios of Upheaval Dome formation, it is convenient to numerically evaluate expressions such as those found in *Everett* [1990], *Kauahikaua* [1978], *Ryu et al.* [1970], *Ward &Hohmann* [1987] and *Morrison et al.* [1969] that represent the electric and magnetic fields produced by an electromagnetic source deployed over a layered Earth. The source considered herein is a horizontal electric dipole (HED) source of infinitesimal length but finite moment. The Hankel transforms are evaluated using the *Guptasarma and Singh* [1997] method. The field expressions are evaluated using software written in the Fortran programming language.

Point HED Source

The HED source is similar to a long wire source, but instead of current flowing over the length of a wire, the source is approximated as a point electric dipole of finite moment with negligible length. This point dipole is situated at the boundary (z=0) between the air and the ground at the origin, x=y=0. The HED source description is based on equations and theory in *Ward & Hohmann* [1987] which prescribed a point dipole source deployed over both homogeneous and layered half-spaces and energized in either the frequency or time domain.

Ward & Hohmann [1987] develop the equations representing the electric and magnetic fields from Maxwell's equations in the frequency domain. The following equations are based on their derivation and represent the equations that will be used to evaluate the response of layered geoelectrical models and will be used in the future development of 3-D finite element modeling.

The electric field generated by the HED source contains two components, the E_x component and the E_y component, which are functions of depth z. The E_x component is shown below in Expression (2.1).

$$E_x = \frac{P}{4\pi}\left(\frac{\partial^2}{\partial x^2}\int_0^\infty \left[(1-r_{TM})\frac{u_0}{\hat{y}_0} - (1+r_{TE})\frac{\hat{z}_0}{u_0}\right]\frac{1}{\lambda}J_0(\lambda\rho)d\lambda - \hat{z}_0\int_0^\infty\left[(1+r_{TE})\frac{\lambda}{u_0}\right]J_0(\lambda\rho)d\lambda\right)$$

(2.1)

In this expression, $P = Ids$ where P represents the dipole moment of the HED in which I is the current and ds is the length of the dipole. The length ds is infinitesimally small and the current I is sufficiently large such that the product Ids is finite. The terms r_{TM} and r_{TE} represent reflection coefficients for the source decomposed into transverse electric (TE) and transverse magnetic (TM) modes. For the scenarios encountered within this project, the low-frequency approximation has been used due to the large depth of the target salt layer, neglecting the displacement current. The reflection coefficients are represented below in the Expressions (2.2) and (2.3).

$$r_{TM} \approx \frac{u_0 - u_1}{u_0 + u_1} \qquad\qquad (2.2)$$

$$r_{TE} \approx \frac{\lambda - u_1}{\lambda + u_1} \qquad\qquad (2.3)$$

The terms u_0 and u_1 are defined as $u_0 = \sqrt{\lambda^2 + \mu_0\sigma_0 i\omega}$ and $u_1 = \sqrt{\lambda^2 + \mu_0\sigma_1 i\omega}$ where $\omega = 2\pi f$ is the angular frequency of the oscillating source, while $\rho = \sqrt{x^2 + y^2}$. The variables $\hat{y}_0$ and $\hat{z}_0$ are defined as $\hat{y}_0 = i\omega\epsilon_0$ and $\hat{z}_0 = i\omega\mu_0$ where ϵ_0 and μ_0 are the electrical permittivity of free space and the magnetic permeability of free space, respectively. In this solution, $\hat{y}_0$ can be approximated as equal to 0 as this solution is concerned with the diffusion process of controlled source EM induction due to the large target depth, rather than the wave-propagation process of

7

ground-penetrating radar. Deriving the equation further, using Bessel function derivative

formulas it is possible to represent the electric field in the x direction as Expression (2.4).

$$E_x = \frac{P}{4\pi}\left(-\int_0^\infty \left[(2)\frac{u_1}{\sigma_1} - (1 + r_{TE})\frac{\hat{z}_0}{u_0}\right]\frac{y^2 - x^2}{\rho^3} J_1(\lambda\rho)d\lambda + \int_0^\infty \left[(2)\frac{u_1}{\sigma_1} - (1 + \right.\right.$$

$$\left.\left. r_{TE})\frac{\hat{z}_0}{u_0}\right]\frac{\lambda x^2}{\rho^2} J_0(\lambda\rho)d\lambda - \hat{z}_0 \int_0^\infty \left[(1 + r_{TE})\frac{\lambda}{u_0}\right] J_0(\lambda\rho)d\lambda\right) \tag{2.4}$$

The electric field in the y direction can also be represented in a similar matter as Expressions

(2.1) and (2.4), and is represented below in Expression (2.5)

$$E_y = \frac{P}{4\pi}\frac{\partial}{\partial x}\left(-\frac{y}{\rho}\int_0^\infty \left[(1 - r_{TM})\frac{u_0}{\hat{y}_0} - (1 + r_{TE})\frac{\hat{z}_0}{u_0}\right] J_1(\lambda\rho)d\lambda\right) \tag{2.5}$$

Using the chain rule to differentiate the product $J_1(\lambda\rho)/\rho$, Expression (2.5) can be represented as

Expression (2.6).

$$E_y = \frac{Py}{4\pi}\left(\int_0^\infty \left[(2)\frac{u_1}{\sigma_1} - (1 + r_{TE})\frac{\hat{z}_0}{u_0}\right]\frac{2x}{\rho^3} J_1(\lambda\rho)d\lambda + \int_0^\infty \left[(2)\frac{u_1}{\sigma_1} - (1 + r_{TE})\frac{\hat{z}_0}{u_0}\right]\frac{\lambda x}{\rho^2} J_0(\lambda\rho)d\lambda\right)$$

$$\tag{2.6}$$

It should be noted, however, that in this solution the electric field in the y direction is equal to 0

if the receiver is placed on the surface along the x-axis (i. e. $y = z = 0$).

The magnetic fields for an HED source are also represented as components in the x and y

direction and are written below in Expressions (2.7) and (2.8).

$$H_x = \frac{P}{4\pi}\frac{\partial}{\partial x}\left(-\frac{y}{\rho}\int_0^\infty [(r_{TM} + r_{TE})]e^{u_0 z} J_1(\lambda\rho)d\lambda\right) \tag{2.7}$$

$$H_y = \frac{P}{4\pi}\left(-\frac{\partial}{\partial x}\frac{x}{\rho}\int_0^\infty [(r_{TM} + r_{TE})]e^{u_0 z} J_1(\lambda\rho)d\lambda - \int_0^\infty (1 - r_{TE}) e^{u_0 z}\lambda J_0(\lambda\rho)d\lambda\right) \tag{2.8}$$

$$H_z = \frac{P}{4\pi}\frac{y}{\rho}\left(\int_0^\infty [(1 + r_{TE})]e^{u_0 z}\frac{\lambda^2}{u_0} J_1(\lambda\rho)d\lambda\right) \tag{2.9}$$

The x and y magnetic field components can be expanded in the same way as the electric field components were expanded in Expressions (2.4) and (2.6). The final forms that are used in the numerical modeling code are represented below as Expressions (2.9) and (2.10).

$$H_x = \frac{Py}{4\pi}\left(-\int_0^\infty [(r_{TM} + r_{TE})]e^{u_0 z}\frac{2x}{\rho^3}J_1(\lambda\rho)d\lambda + \int_0^\infty (r_{TM} + r_{TE})\,e^{u_0 z}\frac{\lambda x}{\rho^2}J_0(\lambda\rho)d\lambda\right) \quad (2.9)$$

$$H_y = \frac{P}{4\pi}\left(-\int_0^\infty [(r_{TM} + r_{TE})]e^{u_0 z}\frac{y^2 - x^2}{\rho^3}J_1(\lambda\rho)d\lambda + \frac{1}{\rho^2}\int_0^\infty (r_{TM} + r_{TE})\,e^{u_0 z}\frac{\lambda x^2}{\rho^2}J_0(\lambda\rho)d\lambda - \right.$$

$$\left.\int_0^\infty (1 - r_{TE})\,e^{u_0 z}\lambda J_0(\lambda\rho)d\lambda\right) \quad (2.10)$$

Layered Solution

In order to convert the response of the homogeneous half space into that of a layered earth, it is necessary to modify Expressions 2.2 and 2.3 to account for an upward recursion taking the electrical conductivity within each of the layers into account. These equations are modified below in Expressions 2.11 and 2.12, as shown in *Ward & Hohmann* [1987].

$$r_{TE} = \frac{Y_0 - \hat{Y}_1}{Y_0 + \hat{Y}_1} \quad (2.11)$$

$$r_{TM} = \frac{Z_0 - \hat{Z}_1}{Z_0 + \hat{Z}_1} \quad (2.12)$$

The relations for the quantities found in Expression 2.11 are given by the recursion below.

$$\hat{Y}_n = Y_n \quad (2.13)$$

$$Y_n = \frac{u_n}{\hat{z}_n} \quad (2.14)$$

$$\hat{Y}_n = Y_n \frac{\hat{Y}_{n+1} + Y_n \tanh(u_n h_n)}{Y_n + \hat{Y}_{n+1}\tanh(u_n h_n)} \quad (2.15)$$

In this solution, $\hat{z}_n$ is equal to $\hat{z}_0$ as μ is approximated as μ_0 in all layers due to the absence of magnetic material. The terms for Expression 2.12, corresponding to the transverse magnetic recursion coefficient, are defined below.

$$\hat{Z}_n = Z_n \tag{2.16}$$

$$Z_n = \frac{u_n}{\hat{y}_n} \tag{2.17}$$

$$\hat{Z}_n = Z_n \frac{\hat{Z}_{n+1} + Z_n \tanh(u_n h_n)}{Z_n + \hat{Z}_{n+1} \tanh(u_n h_n)} \tag{2.18}$$

In Expression 2.17, it is important to note that $\hat{y}_n$ can be represented as σ_n as $\hat{y} = \sigma + i\omega\epsilon_0$ because, as already established, the second term is approximated as 0, leaving σ. Substituting these expressions into the original example, it is possible to develop a solution for the electric field response of the layered earth. This expression is defined below as E_x^{anom}.

$$E_x^{anom} = \frac{P}{4\pi}\left(-\int_0^\infty \left[(2)\hat{z}_1 - (1 + r_{TE})\frac{\hat{z}_0}{u_0}\right]\frac{y^2 - x^2}{\rho^3} J_1(\lambda\rho)d\lambda + \int_0^\infty \left[(2)\hat{z}_1 - (1 + \right.$$

$$\left. r_{TE})\frac{\hat{z}_0}{u_0}\right]\frac{\lambda x^2}{\rho^2} J_0(\lambda\rho)d\lambda - \hat{z}_0 \int_0^\infty \left[(1 + r_{TE})\frac{\lambda}{u_0}\right] J_0(\lambda\rho)d\lambda\right) \tag{2.19}$$

This solution is nearly identical to the half-space E_x expression, however, $\frac{u_1}{\sigma_1}$ is replaced by the layered-earth equivalent $\hat{z}_1$, as well as accounting for the substitution of Expressions 2.11 and 2.12 for r_{TE} and r_{TM} in Expression 2.4.

CHAPTER III

RESULTS

Topography and Stratigraphy

Using elevation data from the Shuttle Radar Topography mission [*Farr,* 2007], a

topographic model of Upheaval Dome has been constructed, as displayed in two perspectives in
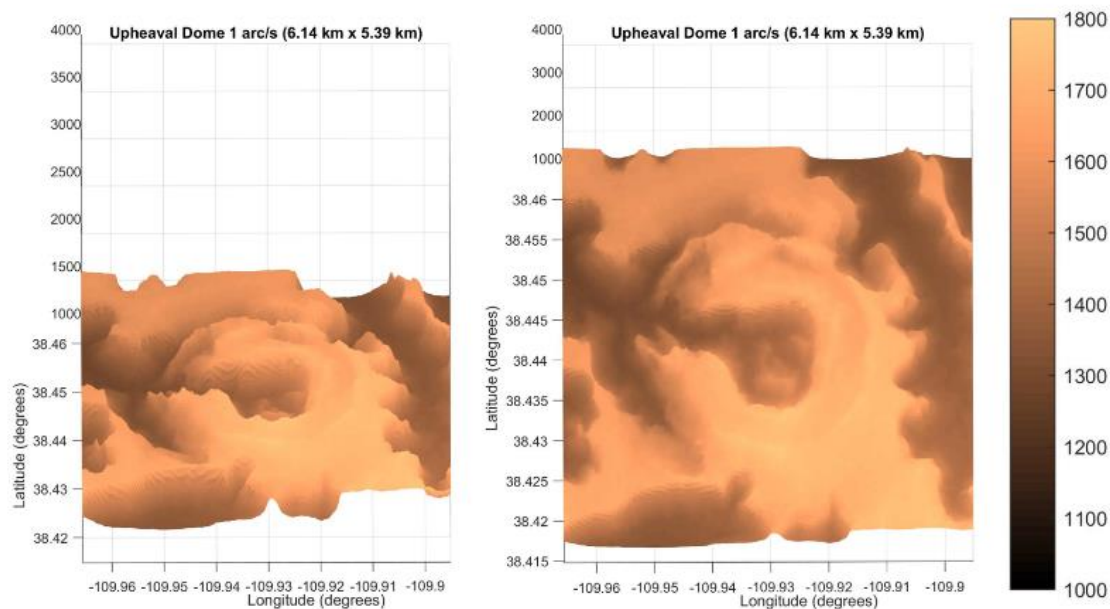
Figure 3.1.

Figure 3.1. Topography of Upheaval Dome. Elevation is in m above the sea level datum.

The parameters selected for the subsurface layer thicknesses and electrical conductivity are

shown in Table 3.2. The layer thickness are based on averaged thicknesses of geological strata as

found in *Jackson* [1998]. Estimated conductivity is averaged across all layers within a group and

is based on textbook values of the corresponding lithologies [*Telford et al.*, 1990]. For the early

stages of the modeling exercises described herein, the estimated electrical conductivities of the

layers above the Paradox Formation were averaged together into a single layer with an electrical

conductivity of 0.003 S/m. This layer resides above a basal layer representing the Paradox

formation, which has a presumed electrical conductivity of 0.0001 S/m. The representation of the

actual multi-layered structure into two representative layers is done for ease in computing the

CSEM response.

Unit	Layer Thickness (m)	Estimated Conductivity (S/m)
Navajo Sandstone	120	0.001
Kayenta Formation	70	0.005
Wingate Sandstone	90	0.001
Chinle Formation	110	0.001
Moenkopi Formation	100	0.002
Black Box Dolomite and Cutler Group	380	0.01
Honaker Trail Formation	360	0.002
Paradox Formation	700	0.0001

Table 3.2. Parameters of Upheaval Dome Stratigraphy. Estimated conductivity is based on the type of sediments that are present in the geological formations [*Jackson*, 1998].

Gravity Data

A gravity survey completed by *Joesting and Plouff* [1958] revealed a central high

Bouguer anomaly which was interpreted by the authors to be the result of either uplifted

basement rock or an igneous intrusion. Using data from the University of Texas, El Paso

Regional Geospatial Service Center, [*Aldouri et.al*, 2013] the Bouguer and free air anomalies are

plotted below (Figure 3.3a and 3.3b, respectively).
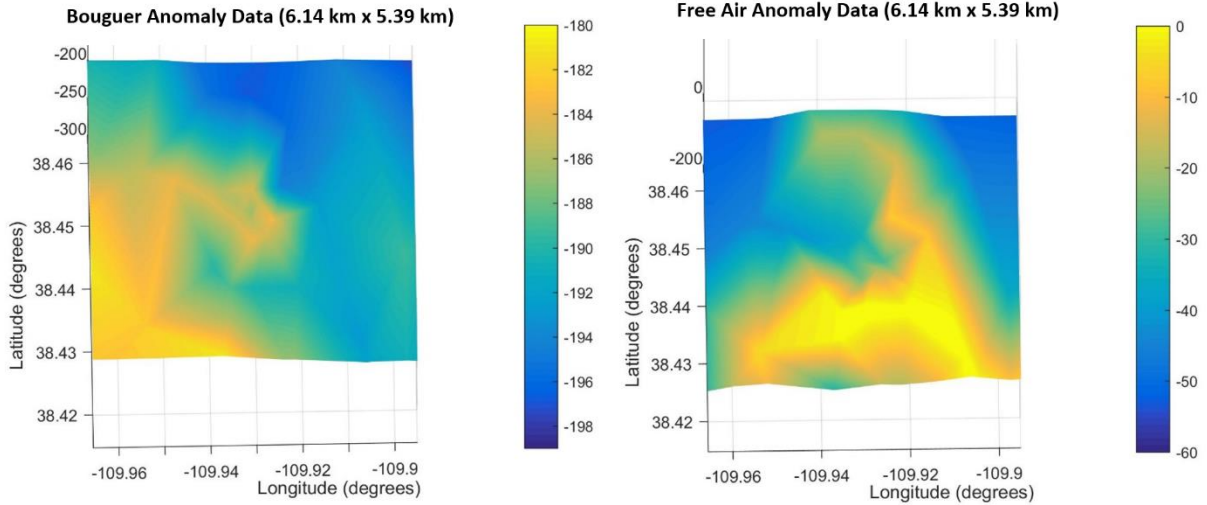
Figures 3.3a and 3.3b. Bouguer and Free Air Anomalies of Upheaval Dome. Figure 3.3a (left) represents Bouguer anomaly reduced to average background crustal density. Figure 3.3b (right) represents the free air anomaly. A prominent high-amplitude anomaly appears in the center of Figure 3.3a.

The high-amplitude anomaly depicted in Figure 3.3a is inconsistent with the theory of upwelling salt originating below the surface. The central high instead indicates higher density material, which is not consistent with the low density Paradox salt formation. Additionally, in comparison to the regional-scale Bouguer anomaly displayed in Figure 3.4, Upheaval Dome is located on the edge of a region of higher density.
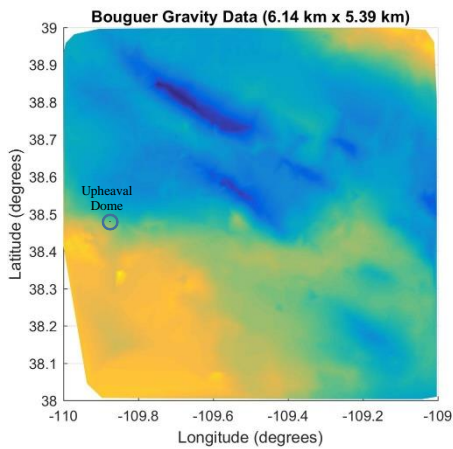
Figures 3.4. Regional Bouguer Gravity Anomaly. In Figure 3.4 Upheaval Dome is shown as a plotted circle.

The low, NW-SE trending Bouguer anomalies in Figure 3.4 correspond to regional outcrops of the Paradox salt layer, as depicted in maps of the area. The regional high-amplitude

anomaly zones caused by denser material is a further example of inconsistency of the Upheaval

Dome site with the salt diapir theory.

E_x Solution and Comparison to *Streich* [2016]

Using the equations developed from *Ward & Hohmann* [1987] and described in the

previous chapter, a computer implementation of the electric field in the x direction was

developed using the Fortran programming language. The result was compared to the

corresponding *Streich* [2016] point dipole implementation in the x direction. The parameters of

the geologic scenarios evaluated in *Streich* [2016] are depicted in Figure 3.5.
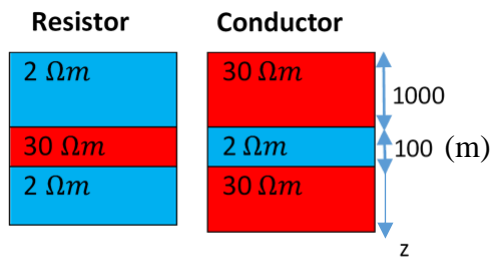

Figure 3.5 Geometry of *Streich* [2016] Geologic Scenarios. This figure is based off of an original figure providing a resistive and conductive layer scenario in *Streich* [2016].

Using the same parameters as *Streich* [2016], code developed from the point dipole solution

equations in *Ward & Hohmann* [1987] was evaluated against the results obtained by *Streich*

[2016]. The results of this comparison is shown in Figures 3.6a and 3.6b.

14
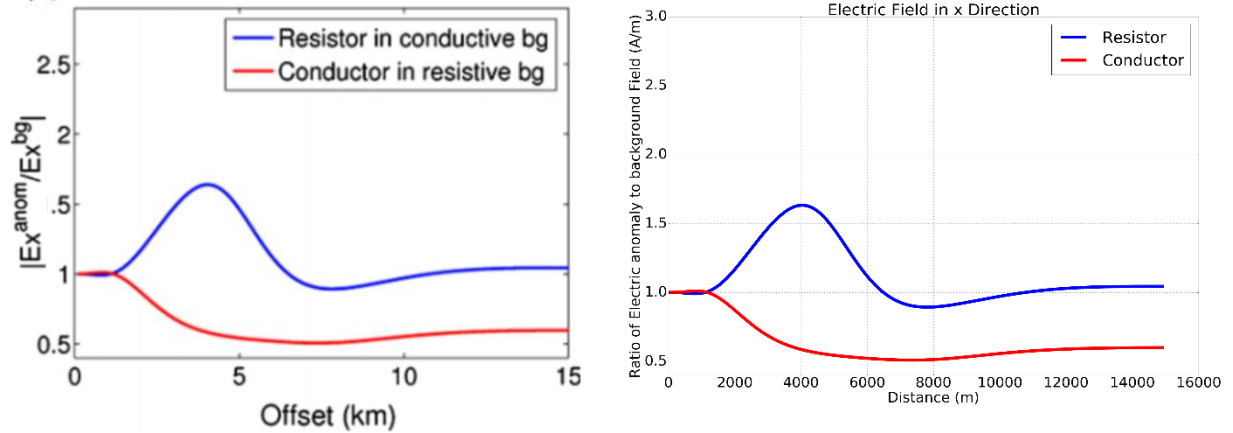
Figures 3.6a and 3.6b. Comparison with *Streich* [2016]. Figure 3.6a (left) is the original graph taken from *Streich* [2016]. Figure 3.6b (right) is the developed code graphed using the same parameters as Figure 3.6a. The y axis represents the magnitude, or anomalous response of the electric field in the x direction, the ratio of the layered solution to the homogenous half space. The x axis represents the transmitter-receiver distance. The resistor is calculated using a 0.2 Hz frequency and the conductor is calculated using a 1 Hz frequency.

Figures 3.6a and 3.6b show an excellent agreement using the same parameters as *Streich* [2016], indicating that the code developed is accurate for modeling the CSEM response of these geologic scenarios.

Evaluation of Upheaval Strata with Variable Salt Depth

Using the code developed and checked against *Streich* [2016], Figure 3.7a depicts a graph representing the magnitude of the signal picked up by an inline electric-field receiver. Different curves represent models that include the Paradox salt layer at various depths. Figure 3.7b is a diagram of the geologic scenario used to construct the graph.
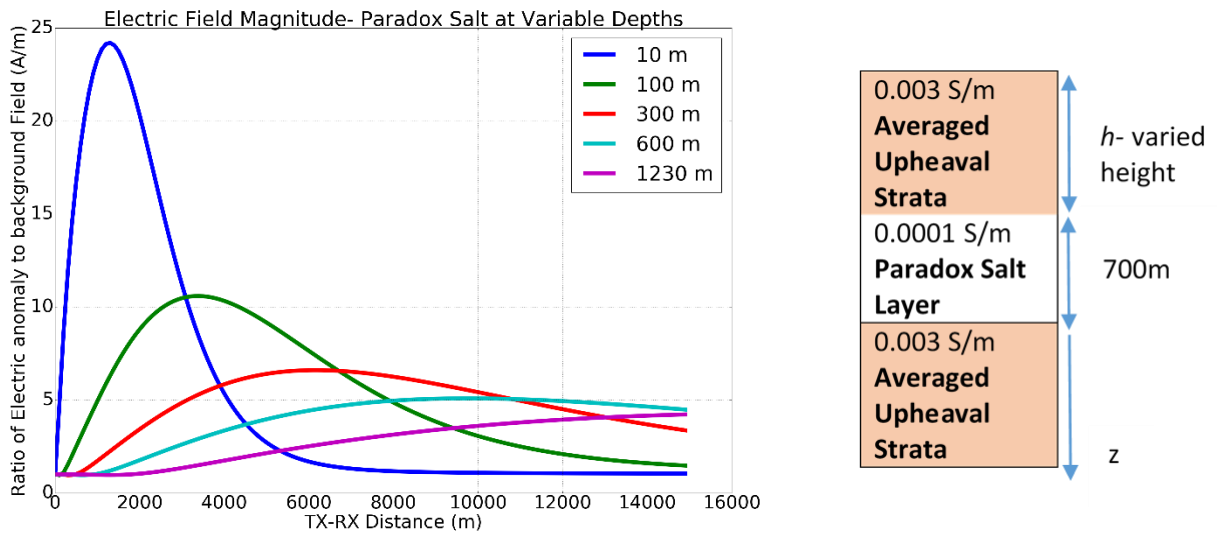
Figure 3.7a and 3.7b. Paradox Salt at Various Depths. Figure 3.7a (left) represents the magnitude of the electric field response in the x of a variable depth Paradox salt layer, calculated using a frequency of 1 Hz. Figure 3.7b (right) is the geologic scenario evaluated with the first layer varying in height from 10 m to 1230 m, the estimated true depth of the Paradox formation.

The variable depths to salt are designed to span the possible theories on the origin of Upheaval

Dome. A shallow salt depth such as 10 m is a representation of the salt diapir theory, in which

salt should be present near the surface. A moderate depth to salt such as 100-300 m is intended

as an estimation for the pinched-off salt diapir theory. The 1230 m depth represents the

geological structure that is expected from a meteorite impact origin of Upheaval Dome. The

optimal placement of transmitter-receivers is determined by the maximum signal so as to receive

the strongest response from the salt layer. Thus, an ideal transmitter-receiver distance for the 10

m scenario would be ~1600 m at 1 Hz.

CHAPTER IV

CONCLUSION

Starting from the governing Maxwell equations, as found in *Ward & Hohmann* [1987], *Everett* [1990], *Kauahikaua* [1978], *Ryu et al.* [1970], and *Morrison et al.* [1969], a point dipole source solution for the in-line electric field was developed and the magnitude of the anomaly calculated and checked against equivalent responses presented in *Streich* [2016]. Through the use of the developed Fortran software, it is possible to develop an experimental design of the ideal transmitter-receiver distance that would optimize resolution of the depth to the Paradox salt layer, a parameter of vital importance in distinguishing between the various proposed scenarios of Upheaval Dome formation. Future work will entail extending the modeling from a point dipole to a long-wire solution, and developing 3-D responses of the various geologic scenarios, including the irregular terrain, using finite element analysis. The eventual goal of this project is to conduct a long wire CSEM survey at Upheaval Dome with the acquisition parameters set through further experimental design and then to compare the field data to the calculated forward models and, ultimately, to use the CSEM results to constrain geological theories of Upheaval Dome formation.

REFERENCES

Al Douri, R., Bustillos, J. G., Flores, M. A. (2013). Regional Geospatial Service Center, University of Texas, El Paso

Baars, D. L., (2000). Geology of Canyonlands National Park: In Geology of Utah's Parks and Monuments, Sprinkel, D.A., Chidsey, T. C., and Anderson, P. B., editors, Utah *Geological Association Publication*, v. 28, pp. 61-83.

Buchner, E. & Kenkmann, T., (2008). Upheaval Dome, Utah, USA: impact origin confirmed. *Geology*, 36, pp. 227-230.

Everett, M.E., (1990). Active Electromagnetics at the Mid-Ocean Ridge: Scripps Institution of Oceanography Library. *UC San Diego: UC San Diego Library – Scripps Collection*, pp.1-139

Farr, T. G. et al., (2007). The Shuttle Radar Topography Mission. *Rev. Geophys*., 45, RG2004, doi:10.1029/2005RG000183.

Guptasarma, D., and Singh, B., (1997). New digital linear filters for Hankel J0 and J1 transforms. *Geophysical Prospecting*, v.45, pp. 745-762.

Jackson, M.P.A., Schulz-Ela, D.D., Hudec, M.R., Watson, I.A., and Porter, M.L., (1998). Structure and evolution of Upheaval Dome: a pinched-off salt diapir. *Geological Society of America Bulletin*, v. 110, pp. 1547–1573.

Joesting, H. R., and Plouff, Donald, (1958). Geophysical studies of the Upheaval Dome area, San Juan County, Utah. *Intermountain Assoc. Petroleum Geologists*, 9th Ann. Field Conference, Paradox Basin, pp. 86–92.

Juhlin, C. and Pedersen, L.B., (1987). Reflection seismic investigations of the Siljan impact structure, Sweden. *Journal of Geophysical Research: Solid Earth (1978–2012)*, v. 92(B13), pp.14113-14122.

Kauahikaua, J., (1978). Electromagnetic Fields about a Horizontal Electric Wire Source of Arbitrary Length. *Geophysics*, v. 43, pp. 1019-1022.

Kanbur, Z., Louie, J.N., Chávez-Pérez, S., Plank, G., and Morey, D., (2000). Seismic reflection study of Upheaval Dome, Canyonlands National Park, Utah. *Journal of Geophysical Research–Planets*, v. 105, pp. 9489–9505.

Kriens, B.J., Shoemaker, E.M., and Herkenhoff, K.E., (1999). Geology of the Upheaval Dome impact structure, southeast Utah. *Journal of Geophysical Research*, v. 104, pp. 18,867–18,887.

Morrison, H.F., Phillips, R.J., and O'Brien, D. P., (1969). Quantitative interpretation of transient electromagnetic fields over a layered half-space. *Geophys. Prosp.*, v. 21, pp. l-20.

McKnight, T., (1940). Geology of area between Green and Colorado Rivers, Grand and San Juan Counties, Utah. *U.S. Geol. Surv. Bull.,* 908, 147 pp., 1940.

Poelchau M. H., Kenkmann T. and Kring D. A., (2009). Rim uplift and crater shape in Meteor Crater: the effects of target heterogeneities and trajectory obliquity. *Journal of Geophysical Research,* v. 114, E01006, doi:10.1029/2008JE003235.

Ryu, J., Morrison, H.F., Ward, S.H., (1970). Electromagnetic Fields about a Loop Source of Current. *Geophysics*, v. 35, pp. 862-896.

Trudgill, B.D., (2011). Evolution of salt structures in the northern Paradox Basin: controls on evaporite deposition, salt wall growth and supra-salt stratigraphic architecture. *Basin Research*, *23*(2), pp.208-238.

Streich, R., (2016). Controlled Source Electromagnetic Approaches for Hydrocarbon Exploration and Monitoring on Land. *Surv. Geophys.* v.37, pp. 47-80.

Telford, W.M., Gledart, L.P., Sheriff, R.E., (1990). *Applied Geophysics* (Cambridge University Press, Cambridge, UK), 770 p. Print

Wait, J.R., (1982). *Geo-Electromagnetism* (Academic Press, New York), 268 p. Print

Ward, S.H. and G.W. Hohmann, (1987). Electromagnetic theory for geophysical applications, in *Electromagnetic Methods in Applied Geophysics,* v. 1, Theory, ed. Nabighian, M.N., Society of Exploration Geophysicists, Tulsa, OK., 131-311.